

**THE PHOTOCHEMICAL REFLECTANCE INDEX FROM DIRECTIONAL  
CORNFIELD REFLECTANCES: OBSERVATIONS AND SIMULATIONS**

[Research Paper]

Yen-Ben Cheng<sup>1,\*</sup>, Elizabeth M. Middleton<sup>2</sup>, Qingyuan Zhang<sup>3</sup>, Lawrence A. Corp<sup>4</sup>,  
Jonathan Dandois<sup>5</sup>, and William P. Kustas<sup>6,a</sup>

<sup>1</sup>Earth Resources Technology, Inc., Laurel, MD 20707, USA

<sup>2</sup>Biospheric Sciences Laboratory, National Aeronautics and Space Administration/Goddard Space  
Flight Center, Greenbelt, MD 20771, USA

<sup>3</sup>Universities Space Research Association, Columbia, MD 21044, USA

<sup>4</sup>Sigma Space Corporation, Lanham, MD 20706, USA

<sup>5</sup>Department of Geography and Environmental Systems, University of Maryland Baltimore  
County, Baltimore, MD 21250, USA

<sup>6</sup>Hydrology and Remote Sensing Laboratory, USDA Agricultural Research Service, Beltsville,  
MD 20705, USA

\*Corresponding author:

Code 618, NASA Goddard Space Flight Center, Greenbelt, MD 20771, USA

Tel: +1 (301) 614-6636; Fax: +1 (301) 614-6695

Email: Yen-Ben.Cheng@nasa.gov

<sup>a</sup>USDA is an equal opportunity provider and employer

1 **ABSTRACT**

2           The two-layer Markov chain Analytical Canopy Reflectance Model (ACRM) was linked  
3 with *in situ* hyperspectral leaf optical properties to simulate the Photochemical Reflectance Index  
4 (PRI) for a corn crop canopy at three different growth stages. This is an extended study after a  
5 successful demonstration of PRI simulations for a cornfield previously conducted at an early  
6 vegetative growth stage. Consistent with previous *in situ* studies, sunlit leaves exhibited lower  
7 PRI values than shaded leaves. Since sunlit (shaded) foliage dominates the canopy in the  
8 reflectance hotspot (coldspot), the canopy PRI derived from field hyperspectral observations  
9 displayed sensitivity to both view zenith angle and relative azimuth angle at all growth stages.  
10 Consequently, sunlit and shaded canopy sectors were most differentiated when viewed along the  
11 azimuth matching the solar principal plane. These directional PRI responses associated with  
12 sunlit/shaded foliage were successfully reproduced by the ACRM. As before, the simulated PRI  
13 values from the current study were closer to *in situ* values when both sunlit and shaded leaves  
14 were utilized as model input data in a two-layer mode, instead of a one-layer mode with sunlit  
15 leaves only. Model performance as judged by correlation between *in situ* and simulated values  
16 was strongest for the mature corn crop ( $r = 0.87$ ,  $RMSE = 0.0048$ ), followed by the early  
17 vegetative stage ( $r = 0.78$ ;  $RMSE = 0.0051$ ) and the early senescent stage ( $r = 0.65$ ;  $RMSE =$   
18  $0.0104$ ). Since the benefit of including shaded leaves in the scheme varied across different  
19 growth stages, a further analysis was conducted to investigate how variable fractions of  
20 sunlit/shaded leaves affect the canopy PRI values expected for a cornfield, with implications for  
21 remote sensing monitoring options. Simulations of the sunlit to shaded canopy ratio near 50/50  
22  $\pm 10$  (e.g., 60/40) matching field observations at all growth stages were examined. Our results

23 suggest in the importance of the sunlit/shaded fraction and canopy structure in understanding and  
24 interpreting PRI.

25

26 ***Highlights:***

27     ➤ Demonstrating PRI responses to illumination conditions and viewing geometry at leaf  
28         and canopy level.

29     ➤ Validating the capability of the two-layer Analytical Canopy Reflectance Model for PRI  
30         simulations in a cornfield at different growth stages.

31     ➤ Investigating how canopy structure associated with variable fraction of sunlit/shaded  
32         leaves affect the PRI values.

33

34 ***Keywords:*** hyperspectral, two-layer Analytical Canopy Reflectance Model (ACRM),  
35 photochemical reflectance index (PRI), cornfield

36

## 37 1. INTRODUCTION

38 Remotely sensed spectral bio-indicators have the potential to play a critical role in  
39 monitoring and modeling processes in time and space for our Earth's ecosystems, including the  
40 exchange of carbon between the biosphere and the atmosphere. This is because uncertainties  
41 exist in how ecosystems will function and what feedbacks to expect, especially under  
42 disturbances induced by the changing climate (Garbulsky et al., 2011; Middleton et al., 2011).  
43 One of the widely used concepts to model carbon assimilation by plants is the light use  
44 efficiency (LUE) model (Monteith, 1972; Monteith, 1977). This approach describes carbon  
45 assimilation, in the form of gross or net primary productivity (GPP, NPP), as the product of the  
46 absorbed photosynthetically active radiation (APAR) and LUE. Previous studies have shown  
47 that LUE can vary based on vegetation type, environmental conditions, and temporal resolution  
48 of the observations (Anderson et al., 2000; Garbulsky et al., 2011; Gower et al., 1999; King et  
49 al., 2011; Middleton et al., 2011; Peñuelas et al., 2011).

50 The importance of accurate LUE estimation has been emphasized in recent studies (e.g.,  
51 Lin et al., 2011; Peñuelas et al., 2011), reporting that errors in LUE are a major contributor to  
52 biases in annual carbon assimilation estimates. Current tools and methods developed for LUE  
53 estimation usually utilize a look-up table of maximum possible LUE, which is then downscaled  
54 by an adjustment coefficient determined using meteorological data (e.g., air temperature and  
55 VPD) to account for non-optimal environmental effects (Law and Waring, 1994; Mahadevan et  
56 al., 2008; Prince and Goward, 1995; Xiao et al., 2004). This approach is used for the satellite  
57 data product available from the Terra and Aqua Moderate Resolution Imaging  
58 Spectroradiometers (MODIS), the MOD17 GPP product (Heinsch et al., 2003; Heinsch et al.,  
59 2006). However, with this approach, errors are usually introduced into LUE estimates due to

60 uncertainties about the fixed values within the look-up table and the meteorological data used for  
61 scaling factors. Moreover, these meteorological data usually have a much larger footprint than  
62 the area of interest, and hence, are not always representative for local LUE (Middleton et al.,  
63 2011). On the other hand, a spectral bio-indicator directly derived from vegetation optical  
64 properties has been shown capable of providing useful estimates of LUE without needing  
65 ancillary information or relying on meteorological data (Garbulsky et al., 2011; Hall et al., 2011;  
66 Huemmrich et al., 2009; Middleton et al., 2009; Middleton et al., 2011; Peñuelas et al., 2011).

67         The LUE of plants is closely linked to the reversible photoprotective responses of the  
68 foliar xanthophyll pigment cycle to illumination conditions, especially as induced by saturating  
69 mid-day irradiances. These responses are expressed by a spectral bio-indicator, the  
70 Photochemical Reflectance Index (PRI; (Gamon et al., 1990; Gamon et al., 1992; Gamon et al.,  
71 1997; Peñuelas et al., 1995). This PRI information can be used to model the down-regulation of  
72 photosynthesis (Demmig-Adams and Adams III, 1996). The PRI utilizes a narrow  
73 physiologically active green band centered at 531 nm and a reference band most typically  
74 centered at 570 nm, in the form of a normalized difference index (i.e.,  $[\rho_{531}-$   
75  $\rho_{570}]/[\rho_{531}+\rho_{570}]$ ). The PRI has been increasingly used and examined for its correlation with  
76 LUE across various vegetation types and scales (Cheng et al., 2009; Coops et al., 2010; Filella et  
77 al., 1996; Gamon et al., 1993; Gamon et al., 1992; Gamon et al., 1997; Garbulsky et al., 2011;  
78 Garbulsky et al., 2008; Hall et al., 2011, 2012; Hilker et al., 2011; Hilker et al., 2012; Inoue et  
79 al., 2008; Middleton et al., 2009; Middleton et al., 2011; Nichol et al., 2002; Peñuelas et al.,  
80 1995; Peñuelas and Inoue, 2000; Peñuelas et al., 1997).

81         However, studies have also shown that various factors affect the remote sensing-based  
82 PRI:LUE relationship at canopy or ecosystem scales, including viewing geometry, canopy

83 structure, leaf area index (LAI), soil background, pigment content and shadow fraction (Barton  
84 and North, 2001; Cheng et al., 2009; Drolet et al., 2005; Gamon et al., 2001; Hall et al., 2008;  
85 Hernández-Clemente et al., 2011; Hilker et al., 2008a; Hilker et al., 2008b; Middleton et al.,  
86 2009; Nichol and Grace, 2010; Sims and Gamon, 2002; Sims et al., 2006; Stylinski et al., 2002).  
87 Furthermore, previous studies have also shown the importance of taking both sunlit and shaded  
88 foliage into account to explain PRI behaviors at the canopy level, since sunlit foliage is more  
89 likely to experience high light-induced environmental stress, and to have lower LUE, and hence,  
90 lower PRI values (Cheng et al., 2009; Cheng et al., 2010; Hall et al., 2008; Hilker et al., 2008b;  
91 Middleton et al., 2009; Peñuelas et al., 1995). It follows that we must have more understanding  
92 about the relative roles of sunlit and shaded foliage in canopies, and associated canopy structure,  
93 to improve our knowledge regarding PRI:LUE relationships. Radiative Transfer (RT) models  
94 provide a powerful tool to study this topic since they are designed to quantitatively examine  
95 changes in vegetation optical properties with leaf biochemical and canopy biophysical properties  
96 (Cheng et al., 2006; Jacquemoud et al., 1996; Verhoef, 1984; Zarco-Tejada et al., 2003; Zhang et  
97 al., 2011).

98 Canopy PRI was studied for water stress detection using the PROSPECT leaf model  
99 linked with the SAILh and FLIGHT canopy RT models to produce a non-stressed version of the  
100 PRI in two tree-structured orchards and a maize field (Suárez et al., 2009). In a more recent  
101 study, the leaf model LIBERTY was coupled with the canopy model INFORM to study PRI as a  
102 physiological stress indicator in conifer forests (Hernández-Clemente et al., 2011). Both studies  
103 focused on PRI acquired at near nadir angles. Cheng et al. (2010) utilized *in situ* leaf optical  
104 properties coupled with a Markov chain Analytical two-layer Canopy Reflectance Model  
105 (ACRM; (Kuusk, 1995a, b, 2001) to simulate nadir and directional PRI at the canopy level in a

106 cornfield, which was compared and validated with *in situ* canopy PRI observations. That study  
107 showed that ACRM successfully simulated PRI under various viewing geometries for a corn  
108 crop in the early vegetative stage without noticeable environmental stressors present, and  
109 explored how several canopy structure parameters affected PRI values. The ACRM-simulated  
110 PRI showed the best agreement with *in situ* values when the model was run in a two layer  
111 simulation mode, using leaf optical properties from sunlit leaves as the upper layer and shaded  
112 leaves as the lower canopy (Cheng et al., 2010). In the current study, we took a step further to  
113 examine the robustness of the same algorithm to simulate PRI through three different growth  
114 stages for a corn crop, examining early vegetative, fully mature, and senescent canopies. Our  
115 objective was to determine whether the directional PRI responses previously observed for a  
116 young, vigorous canopy also continue to be present throughout the growing season, and to  
117 characterize and evaluate them. We also investigated how the vertical distribution of sunlit and  
118 shaded leaves affect an important structure-related variable, the canopy sunlit/shaded foliage  
119 ratio, and associated canopy PRI values.

120

## 121 **2. Methods**

### 122 **2.1. Study Site and Field Data Collection**

123 During the summer of 2010, field campaigns were conducted on a corn crop (*Zea mays*  
124 L.) in an experimental cornfield at the Optimizing Production Inputs for Economic and  
125 Environmental Enhancement (OPE3) site (39.0304°N, 76.8458°W) maintained by the USDA  
126 Beltsville Agricultural Research Center (BARC) in Beltsville, Maryland, U.S.A. Measurements  
127 were acquired on three dates representing three different growth stages: an early vegetated  
128 canopy when plants had nine fully expanded leaves (V9) and were ~1 m tall on 07/01; a fully

129 mature canopy having 13-15 fully expanded leaves at ~2 m tall in the early reproductive phase  
130 (VT) on 07/15; and an early senescent crop (~2 m tall) at the advanced reproductive development  
131 stage (R4) on 08/09. Canopy and leaf level measurements were taken along a 100-m north-south  
132 direction transect in the middle of the field to minimize disturbance and to maintain  
133 representativeness of the data. Hyperspectral reflectance (~1.5 nm Full Width Half Maximum;  
134 FWHM) was obtained for vegetation at both leaf and canopy levels and on bare soil using an  
135 USB4000 Miniature Fiber Optic Spectrometer (Ocean Optics Inc., Dunedin, FL, USA) with a  
136 bare fiber. *In situ* leaf reflectance observations were acquired directly adjacent to the adaxial leaf  
137 surfaces. The leaves were excised on the next day, and a Li-Cor 1800-12 integrating sphere (Li-  
138 Cor, Lincoln, NE, USA) paired with a spectroradiometer (FieldSpec, ASD Inc., Boulder, CO,  
139 USA) was utilized to determine transmittance from the leaf adaxial surfaces in the laboratory. At  
140 the canopy level, reflectance spectra were acquired at eight different relative azimuth angles ( $\psi$ ,  
141  $0^\circ$  to  $315^\circ$  relative to the sun, at  $45^\circ$  increments) coupled with three different view zenith angles  
142 ( $\theta_v$ )--  $30^\circ$ ,  $45^\circ$ ,  $60^\circ$  (obtained at 1.3, 0.75, 0.44 m above the canopy, respectively, to provide a  
143 consistent center of the field of view). Nadir ( $\theta_v = 0^\circ$ ;  $\psi = 0^\circ$ ) observations were acquired above  
144 the canopy at a height of approximately 1 m. This was accomplished by placing the fiber optics  
145 from a height-adjustable pole-mount, where a custom-made fixture was designed to position the  
146 instrument at a desired view zenith angle and relative azimuth angle. Soil background reflectance  
147 was taken on bare soil also approximately 1 m above the surface at nadir. Measurements were  
148 taken between local time 9 am to 4 pm, during which the solar zenith angle ( $\theta_s$ ) varied between  
149  $16.6^\circ$  and  $51.2^\circ$  across the season. Crop LAI was also measured with a Li-Cor LAI-2000 plant  
150 canopy analyzer (Li-Cor, Lincoln, NE, USA). More detailed information regarding field data  
151 collections can be found in Cheng et al. (2010).

152 NOTE: The mention of trade names of commercial products in this article is solely for the  
153 purpose of providing specific information and does not imply recommendation or endorsement  
154 by the U.S. Department of Agriculture

## 155 2.2. Models and Simulation Methods

156 In this study, the canopy model ACRM (Kuusk, 1995a, b, 2001) was utilized to simulate  
157 PRI. This RT canopy model is equipped with an enhanced Markov chain bidirectional gap  
158 probability function that has been utilized in various studies using forward and inversion modes  
159 to validate and/or to estimate plants biochemical properties at leaf and/or canopy level (Cheng et  
160 al., 2010; Cheng et al., 2006; Fang et al., 2003; Houborg et al., 2009; Houborg et al., 2011). In  
161 our previous study, in which ACRM successfully simulated PRI for a young corn canopy,  
162 ACRM was set to run in its forward mode utilizing *in situ* leaf and soil background spectra to  
163 simulate canopy spectra at various viewing geometry ( $\theta_v$ ,  $\psi$ ) configurations (Cheng et al.,  
164 2010). PRI was derived from the ACRM-simulated canopy reflectance spectra, and compared  
165 with the PRI derived from *in situ* canopy reflectance spectra. In this study, we followed the  
166 procedures presented in Cheng et al. (2010; 2011) and ran the model in two different modes: (i)  
167 with optical properties of sunlit leaves (only) in a single layer, or (ii) with both sunlit and shaded  
168 leaves in two layers, where the shaded layer laid below the sunlit layer. PRI was then derived  
169 from ACRM-simulated spectra and compared, as before, with PRI derived from *in situ* canopy  
170 reflectance spectra for validation. Values of other essential input parameters for the model are  
171 summarized in Table 1. These values came from either ancillary field measurements (e.g., LAI)  
172 or were decided based on previous studies (Cheng et al., 2010; Cheng et al., 2006; Fang et al.,  
173 2003; Houborg et al., 2009; Jacquemoud, 1993; Kuusk, 2001; Zarco-Tejada et al., 2003).

174 In Cheng et al. (2010; 2011), a sensitivity analysis was performed on several canopy  
175 structure parameters to investigate their effects on PRI simulations. The important influence of  
176 LAI on PRI simulations was reported. This study extends our progress and investigates how the  
177 vertical distribution and partitioning of LAI between the sunlit upper and the shaded lower  
178 canopy layers affect PRI simulations. In our earlier studies, when ACRM was set to run in the  
179 one layer mode, the LAI of the upper canopy was assumed to represent the total LAI, or 100%,  
180 such that the LAI fractions in upper/lower layers were 100% and 0% (i.e., 100/0). Likewise,  
181 when ACRM was set to run in the two layer mode, the LAI fractions of the upper and lower  
182 layers were assumed to equal half of the total LAI, (i.e., 50/50). In the current study, a sensitivity  
183 analysis was performed by changing the ratio of sunlit upper/shaded lower layer LAI values in  
184 10% increments from 100/0 (fully sunlit) to 10/90 (mostly shaded).

185

### 186 **3. RESULTS**

#### 187 **3.1. *In situ* Leaf and Canopy Observations**

188 Leaf-level PRI values derived from *in situ* leaf reflectance are summarized in Figure 1 as  
189 mean  $\pm$  standard error (SE). PRI for sunlit leaves consistently exhibited lower values than shaded  
190 leaves on all three dates (ANOVA; n=60 for each day; 07/01, p<0.0001; 07/15, p=0.0003; 08/09,  
191 p=0.001). Average PRI values varied from -0.009 to +0.005 for sunlit leaves, and consistently  
192 exhibited negative values in the afternoons throughout the growing season. In contrast, mean  
193 PRI values for shaded leaves were always positive, varying from +0.002 to +0.022. PRI also  
194 showed higher mean values in the morning (AM) than in the afternoon (PM) on the two dates  
195 dominated by green foliage before senescence, especially for sunlit leaves (n=30, p<0.001 for  
196 both days). Among the three growth stages, PRI values were significantly higher for shaded

197 leaves (AM and PM) and sunlit leaves (AM) in the mature VT canopy (July 15) than on either  
198 the early (V9) or later season (R4) growth stages (n=30, p<0.0001). At senescence, no clear  
199 differences were observed between the morning and the afternoon (n=30, p=0.6 for sunlit;  
200 p=0.48 for shaded leaves) but the pattern of higher PRI values for shaded vs. sunlit leaves was  
201 maintained.

202 At the canopy level, *in situ* PRI values were plotted as mean  $\pm$  SE against viewing  
203 geometry ( $\theta_v$ ,  $\psi$ ) for the three growth stages in Figure 2. The pattern obtained at leaf level (Fig.  
204 1) for higher PRI at the VT stage (July 15) was maintained at the canopy level (-0.02 to +0.01)  
205 when viewed over a range of view angles ( $\theta_v$ ,  $0^\circ$ ,  $30^\circ$ ,  $45^\circ$ , and  $60^\circ$ ). Lower PRI values (-0.03 to  
206 -0.01) occurred at both early (Fig.2, 07/01) and late stages (Fig.2, 08/09), which were similar in  
207 their PRI responses at the smaller view zenith angles ( $0^\circ$ , n=48, p=0.44;  $30^\circ$ , n=128, p=0.16;  $45^\circ$ ,  
208 n=128, p=0.06) as compared to mid-season VT stage. However, early and late growth stages  
209 were differentiated by PRI values obtained at the extreme view,  $\theta_v = 60^\circ$  (early > late, n= 128,  
210 p=0.0011). PRI values at all azimuth positions increased as a function of  $\theta_v$ . For example,  
211 increases in the mean PRI at the coldspot ( $\psi = 180^\circ$ ) for the VT canopy were:  $-0.003 \pm 0.005$  at  
212  $30^\circ$ ,  $0.0 \pm 0.003$  at  $45^\circ$ , and  $+0.009 \pm 0.006$  at  $60^\circ$ . This contrasts with the negative PRI obtained at  
213 nadir ( $-0.02 \pm 0.003$ ), which would be interpreted as indicating greater physiological stress than  
214 was determined at any other view. The general pattern exhibited for all measurement geometries  
215 ( $8 \psi$  at  $3 \theta_v$ ) was for PRI values to be lower when  $\theta_v$  was close to  $0^\circ$  and highest when  $\psi \approx 180^\circ$   
216 at any  $\theta_v$ , highlighting the dependence on viewing geometries. Together, these results (Figs. 1,  
217 2) demonstrate the influence of diurnal and directional effects on PRI values retrieved from a  
218 cornfield.

### 219 3.2. ACRM-simulated PRI

220 Reflectance spectra were simulated as output from the ACRM. PRI values were  
221 calculated from those and compared with *in situ* PRI for validation purposes in Figure 3, where  
222 PRI values from both field measurements and simulations were plotted against  $\theta_v$  and  $\psi$  (Fig. 3  
223 a,c,e). ACRM-simulated PRI successfully captured the responses that *in situ* PRI exhibited to  $\theta_v$   
224 and  $\psi$  (Fig. 3 a,c,e), producing lower values when  $\psi$  was close to  $0^\circ$  and higher values when  $\psi$   
225 was close to  $180^\circ$  at all  $\theta_v$  on all three observation days. When the simulations were performed  
226 with sunlit leaves only, considerable underestimations as compared to *in situ* PRI values were  
227 observed (Fig. 3 a,c,e). The PRI underestimations were more pronounced on the young V9 crop  
228 (July 1) and the senescent R4 crop (August 9), but also occurred at smaller  $\theta_v = 30^\circ$  for the  
229 mature VT crop. On the contrary, the differences between simulated and *in situ* values were  
230 much smaller, and in most cases not significant, when the simulation included both sunlit and  
231 shaded leaves (Figure 3a,c,e). Correlations between simulated vs. measured values are presented  
232 in Fig. 3b,d,f (panels on the right). The fully mature VT canopy (July 15, Fig. 3d) exhibited the  
233 highest correlation between *in situ* values and simulations under both scenarios: when both  
234 sunlit and shaded leaves were included ( $r = 0.87$ ) and when only sunlit leaves were used ( $r =$   
235  $0.84$ ). The comparisons for the V9 canopy were also strong ( $r = 0.78$ , both sunlit and shaded  
236 leaves;  $r = 0.80$ , sunlit leaves only), although the sunlit (only) set is clearly offset from the 1:1  
237 line. Results were weaker in the senescent R4 stage ( $r = 0.65$ , both sunlit and shaded leaves;  $r =$   
238  $0.52$ , sunlit leaves only), with high variability-- especially for the sunlit dataset. Therefore,  
239 simulated PRI using both sunlit and shaded leaves (Fig. 3) yielded better correspondence (closer  
240 to the 1:1 line) on all three dates than simulations with only sunlit leaves. Statistics of  
241 comparisons between *in situ* and simulated PRI are summarized in Figure 4. For all three days,

242 when compared with *in situ* values, simulated PRI using both sunlit and shaded leaves (Fig. 4)  
243 generated significantly smaller root mean square error (RMSE) than simulations with sunlit  
244 leaves only (Fig. 4). Among the three days, simulated PRI showed the best agreement with *in*  
245 *situ* values at the VT stage, as evidenced by higher correlation coefficients ( $\geq 0.84$ ) and smaller  
246 RMSEs ( $\leq 0.0096$ ) when the canopy was mature (Fig. 4).

247 The performance of ACRM-simulated PRI was further examined by calculating the  
248 difference from *in situ* values, which is summarized in Figure 5. The thick black line displayed in  
249 Fig. 5 indicates no (zero) difference between *in situ* and simulated values. Simulations performed  
250 using only sunlit leaves produced underestimations of field values, as shown by negative values  
251 (Fig. 5a). The largest underestimates ( $\sim 0.03$ ) were obtained at the two smaller view angles, nadir  
252 ( $0^\circ$ ) and  $\theta_v=30^\circ$ . The only simulations with sunlit leaves alone that agreed with field  
253 measurements occurred for  $\theta_v=60^\circ$  in the forward scattering direction ( $\psi = 135^\circ$  to  $270^\circ$ ), for the  
254 fully green and mature mid-season VT canopy (Fig. 5a). When both sunlit and shaded leaves  
255 were used in simulations, the differences were much closer to zero (Fig. 5b), providing better  
256 agreements with *in situ* values under all observation and growth conditions. However,  
257 simulations done using both sunlit and shaded leaves for the VT canopy showed a small positive  
258 bias for part of the  $\psi$  range at all  $\theta_v$ , whereas the differences appeared to scatter around zero at  
259 the other two growth stages (Fig. 5b).

### 260 3.3. Canopy Structure and PRI Simulations

261 The importance of taking optical properties of both sunlit and shaded leaves into account,  
262 as well as their relative proportions in the canopy, expressed as a canopy-level ratio, was further  
263 investigated using the mid-season VT canopy data. Figure 6 shows how the ACRM-simulated  
264 PRI values changed as a function of the sunlit/shaded canopy ratio and viewing geometry, for a

265 corn crop having LAI = 2.48. Columns with lighter shading indicate higher sunlit/shaded  
266 fractions. In the modeling scheme, a higher sunlit/shaded canopy ratio describes a canopy that is  
267 dominated by sunlit leaves, and therefore, optical properties of sunlit leaves influence the  
268 simulated canopy reflectances significantly more. On the contrary, a darker tone (Fig. 6)  
269 indicates lower sunlit/shaded canopy ratios were used to simulate situations where shaded leaves  
270 contributed more to the total canopy reflectance. Clearly, the PRI values obtained at any  $\theta_v$  and  
271  $\psi$  decrease as the sunlit/shaded canopy ratio favors more sunlit foliage (Fig. 6). A lower PRI  
272 value would indicate greater environmental stress, and reduced LUE. Therefore, for the same  
273 canopy LAI and growth stage, different inferences about LUE could be made based on the  
274 observed PRI, depending on viewing geometry and the inherent canopy structure profile. These  
275 results help explain why there have been so many confounding factors that influence the PRI of  
276 canopies that have been reported by various researchers.

277 These simulations were also directly compared with *in situ* PRI values (Figure 7), to  
278 reveal a linear shift away from the 1:1 line for the extreme cases, and displaying a general  
279 underestimation for the full sun (100/0) case, especially at lower PRI values, and a general  
280 overestimation for the mostly shaded (20/80) case. Statistics for the correlation coefficients and  
281 RMSEs are summarized in Figure 8, indicating the highest correlations paired with the lowest  
282 RMSE were associated with two groups in the mid-range (70/30, 60/40). The slope and offset of  
283 the regression lines (Figure 9), show a consistent decline for the slope (parameter “a”) as the  
284 sunlit/shaded canopy ratio increasingly favored more shaded foliage, whereas the offset  
285 (parameter “b”) increased. Since the best agreement between simulations and *in situ* observations  
286 was achieved for a 60/40 ratio, we can assume our field measurements were acquired at or near

287 the 60/40 sunlit/shaded canopy conditions. Thus, our original assumption of a 50/50 ratio was  
288 not the optimal condition for the mature VT canopy in 2010.

289

## 290 **4. Discussion**

291 The PRI was developed to track the reversible changes in the photoprotective xanthophyll  
292 cycle induced by light intensity changes through a diurnal cycle, (Gamon et al., 1992; Peñuelas  
293 et al., 1995). Subsequently, additional environmental stresses have been shown to influence the  
294 pH of the chloroplast stroma, affecting the xanthophylls cycle and associated PRI values, such as  
295 drought and cold temperatures (Demmig-Adams and Adams, 2000; Müller et al., 2001; Pfündel  
296 and Bilger, 1994). Studies have also shown correlations between PRI and other  
297 physiological/morphological changes, for instance, the carotenoids and chlorophyll ratio (Filella  
298 et al., 2004; Sims and Gamon, 2002). In our previous study, we successfully demonstrated that in  
299 *situ* leaf optical properties coupled with ACRM could simulate PRI for a young, homogeneous  
300 corn canopy, still growing and in the vegetative growth stage. Here, we extended our study to  
301 simulate PRI for a corn crop during three different growth stages during the 2010 growing  
302 season.

### 303 **4.1. *In situ* PRI at Leaf and Canopy Level**

304 First of all, the results presented here confirm our previous studies showing that shaded  
305 leaves captured in the coldspot of canopy directional reflectances have higher PRI values than  
306 sunlit leaves (Cheng et al., 2010; Gamon et al., 1990; Middleton et al., 2009; Peñuelas et al.,  
307 1995), and we extended those observations to examine the PRI responses through a growing  
308 season in the same experimental cornfield location as the previous study. Higher PRI values in

309 shaded foliage and canopy sectors indicate that the intensity of xanthophyll-regulated  
310 photoprotection is lower than in sunlit leaves and canopy segments which are more likely to  
311 experience high light stress and exhibit lower PRI values. Furthermore, previous studies have  
312 shown correlations between leaf pigments (e.g. carotenoids/chlorophyll ratio) and PRI and the  
313 changes in PRI values could be related to leaf development and aging during the growing season  
314 (Garbulsky et al., 2011; Peñuelas et al., 2011).

315 Leaf level PRI for the “green” canopies (i.e., the V9 through VT growth stages) exhibited  
316 lower PRI values (i.e., greater stress) during afternoons after several hours of high irradiance  
317 exposure, than for mornings (Fig. 1). This pattern was also observed in our V10 dataset  
318 acquired in the same field in 2008 (Cheng et al., (2010), although the 2008 values were much  
319 higher, implying lower relative stress responses, which were very likely due to an abnormally  
320 wet spring that year. Higher PRI values were also obtained in shaded leaves vs. sunlit leaves in  
321 both morning and afternoon observations in the chlorophyll-dominated growth stages. For the  
322 senescent canopy, however, lower PRI values were found in shaded and sunlit leaves all day  
323 long. These lower mean PRI values for the senescent growth stage discriminated between  
324 shaded and sunlit (shaded > sunlit) but not AM vs. PM due to high variability (Fig. 1).  
325 Nevertheless, the importance of AM vs. PM observations in studying PRI vs. LUE or using PRI  
326 to determine LUE needs to be emphasized. The daily PRI averages followed the expected  
327 pattern: VT > V9 > R4, but the daily variation became large, as compared with either morning  
328 or afternoon observations. On the other hand, considerable error in estimating daily PRI values  
329 would be incurred if only sunlit foliage was considered on any of the dates examined, but  
330 especially for the mature, mid-season VT crop that had the largest sunlit vs. shaded PRI

331 difference. These findings should serve as a caution when utilizing daily average PRI values in  
332 model simulations of LUE at the ecosystem scale.

333 The canopy PRI observations showed substantial dependence on viewing geometry  
334 (Fig. 2), similar to results reported in our previous study (Cheng et al., 2010). PRI values were  
335 higher when the canopy was viewed at larger, oblique  $\theta_v$  since more shaded foliage and less soil  
336 background contamination was captured. Secondly, PRI exhibited higher values when  $\psi$  was at  
337 the coldspot, close to  $180^\circ$  where the shaded dominated the field of view, and lower values when  
338  $\psi$  was close to the hotspot at  $0^\circ$  (broadly including  $45^\circ$ ,  $315^\circ$ ) where it was associated with the  
339 sunlit segment of the canopy (Fig. 2). This is a consistent pattern that has been observed in  
340 multiple years under different conditions for the cornfield and in forests (Hall et al., 2008; Hilker  
341 et al., 2008b; Huemmrich et al., 2009; Middleton et al., 2009). When utilizing spaceborne data,  
342 the observations are not always acquired at nadir (e.g., EO-1 Hyperion, Terra/Aqua MODIS).  
343 Therefore, this confounding effect needs to be addressed to retrieve meaningful information of  
344 plant physiological conditions from non-nadir as well as nadir PRI values. Previous studies  
345 conducted at a Douglas fir forest in British Columbia, Canada, also reported that PRI exhibited  
346 similar dependency to viewing geometry (Hall et al., 2008; Hilker et al., 2008b; Middleton et al.,  
347 2009), and are supported by a recent satellite study using off-nadir directional observations (Hall  
348 et al., 2011; Hilker et al., 2011).

349 PRI values at both leaf and canopy levels expressed less variance (e.g., smaller SE) in  
350 the young, homogeneous, unstressed V9 canopy (Figs. 1,2), with more variability accruing  
351 through the season as the crop aged, weathered, and experienced various unfavorable  
352 environmental conditions.

#### 353 4.2. Simulation Performance and Differences in Previous Study

354 ACRM has been shown to successfully simulate canopy PRI values and their  
355 dependency on viewing geometry with the current 2010 data and with the previous 2008 data.  
356 ACRM was able to deliver believable simulations when both sunlit and shaded leaves were used  
357 (Fig. 3). However, when only sunlit leaves were included in the process, less agreement with  
358 field measurements was achieved and comparisons to *in situ* measurements produced higher  
359 RMSEs due to underestimation. The agreement with *in situ* PRI values was better when the corn  
360 crop was dominated by green foliage from the actively growing, early vegetative through the  
361 mature, reproductive growth stages. When the corn crop approached the senescent stage, ACRM  
362 simulation was satisfactory, but agreed with *in situ* values the least well among our datasets. The  
363 early senescent R4 crop, which had a lower leaf layer in the canopy comprised of brown (dead or  
364 low chlorophyll) leaves coupled with a mixed green/brown upper leaf canopy layer, exhibited  
365 relatively low PRI values (and high stress) in general, especially in the sunlit layer. The  
366 increasing complexity of the foliage distribution at this highly variable stage presents a challenge  
367 for simulations.

368 In our previous study, we showed that using sunlit and shaded leaves in the ACRM  
369 scheme can improve both the correlation and RMSE with *in situ* PRI values (Cheng et al., 2010).  
370 By considering the results from two field studies (2008, 2010), we can conclude that the most  
371 significant benefit of adding shaded leaves as the lower canopy layer in ACRM was to improve  
372 RMSE relative to field observations (see Fig.4 and Cheng et al., 2010). When ACRM was run  
373 in the one layer mode using only the optical properties of sunlit leaves, the simulated PRI  
374 showed satisfactory correlations with *in situ* values but had a significant offset, indicating an  
375 underestimate that could be incorrectly interpreted as a higher than actual physiological stress

376 response. This is an important issue since misinterpretation of PRI values will lead to significant  
377 errors in LUE and GPP estimates. This point was emphasized by calculating the difference  
378 between *in situ* and simulated PRI values for various viewing geometry and dates (Fig. 5) where  
379 simulations performed with only sunlit leaves obviously produced most of the underestimations  
380 as negative values (Fig. 5a). Small  $\theta_v$  (nadir at  $0^\circ$  and  $30^\circ$ ) had larger discrepancies than larger  
381 off-nadir views ( $45^\circ$ ,  $60^\circ$ ), as compared with measurements. This is consistent with our previous  
382 study (Cheng et al., 2010), due in part to less soil background contamination at oblique angles.  
383 Among the three dates, discrepancies between field observations and “sunlit only” simulations  
384 were the smallest for the mature VT canopy (July 15, 2010), especially notable for  $\theta_v = 60^\circ$  (X),  
385 suggesting that at this oblique angle, sunlit leaves might dominate the field of view for a fully  
386 leafed out, green and erectophile canopy. We also note that the benefit of adding a shaded lower  
387 leaf layer for the VT canopy in the ACRM scheme, while advantageous, was less than on the  
388 other dates. This may be because the fully mature crop exhibited more sunlit leaves, greater  
389 canopy closure, and/or a well-developed vertical LAI profile. The latter factor has been shown  
390 to be temporally variant based on the growth stages of corn canopies (Ciganda et al., 2008).

### 391 **4.3. Sunlit/Shaded Canopy Ratio**

392 We tested various cases of variable sunlit/shaded canopy ratios, using our VT mature  
393 canopy dataset, for which the ACRM-simulated PRI values (for a given  $\theta_v$  and  $\psi$ ) were expected  
394 to increase when the sunlit/shaded ratio changed from 100/0 to 10/90. Those simulations (Fig. 6)  
395 duplicated those from the earlier study (Cheng et al. 2010): (1) the highest PRI values occurred  
396 at the coldspot ( $\psi = 180^\circ$ ) and the lowest at the hotspot ( $\psi = 0^\circ$ ); and (2) the PRI values were  
397 higher when  $\theta_v$  increased from  $30^\circ$  to  $60^\circ$ . Therefore, in the ACRM simulations, changes to the

398 sunlit/shaded ratio affected the canopy PRI responses expected, but not the sensitivity to viewing  
399 geometry.

400         However, changes in the canopy structure could affect PRI values, causing  
401 underestimation or overestimation of “true” PRI values. When simulations were done with sunlit  
402 leaves only (100/0 in Fig. 7), most of the data points fell below the 1:1 line, underestimating,  
403 “true” field values. After adding optical properties of shaded leaves in the simulation, even for  
404 the 80/20 case, the data points moved closer to the 1:1 line and generated a ~50% improvement  
405 in RMSE (Fig. 7). On the other hand, when even more shaded leaves than sunlit leaves were  
406 included in the simulation (e.g., 40/60 and 20/80, Fig. 7), the simulated PRI moved up and over  
407 the 1:1 line, and generated higher RMSE due to overestimation. For this dataset, the simulated  
408 60/40 sunlit/shaded canopy ratio appeared to have the best agreement with field measurements,  
409 and indicates that this was the likely field condition at that growth stage in 2010. Since these  
410 simulations used a homogeneous, fixed LAI (at 2.48), the sunlit dominated groups (e.g., 100/0  
411 and 80/20) might indicate relatively more open canopies, made possible by longer stems and/or  
412 wider rows that put space between the leaves (since the number of leaves per plant is fixed).  
413 Likewise, the extreme case for a mostly shaded 20/80 canopy has a more compact, closely  
414 spaced leaf arrangement along a short stem, and/or a closed canopy in narrower rows.

415         Results summarized in Tab. 2 also confirm the importance of adding shaded leaves into  
416 the simulation scheme, since even when using a 80/20 ratio as the input, significant improvement  
417 in RMSE (~30% to 50%) can be achieved. For the mature VT canopy, even though the 60/40  
418 ratio appeared to be optimal by generating the best agreement of the sunlit/shaded ratio to *in situ*  
419 measurements ( $r = 0.87$ ;  $RMSE = 0.0045$ ), the performance using 50/50 was still quite close ( $r =$   
420  $0.87$ ;  $RMSE = 0.0048$ ). Furthermore, after finding that the 50/50 sunlit/shaded ratio was not the

421 optimal value to generate the best simulations for the mature VT canopy, we investigated the  
422 issue for the other two dates in 2010 and one V10 dataset acquired on August 1, 2008 (Tab. 2).  
423 For all three of these other datasets, the 50/50 sunlit/shaded ratio did appear to be optimal for  
424 simulating canopy PRI, based on better statistical performances (higher correlation coefficients  
425 and lower RMSEs). Therefore, while additional canopy structure information might improve  
426 PRI values interpretation and simulation in a cornfield using ACRM, the 50/50 sunlit/shaded  
427 ratio will generate more than satisfactory results for most of the cases.

428         These results indicate that the sunlit/shaded ratio, a structure-based parameter, may  
429 change within a growing season. Therefore, this sensitivity analysis highlights the importance  
430 of canopy structure in simulating and understanding PRI. The implication is that since different  
431 vegetation types have different canopy structures (e.g., forests vs. crops vs. shrubs), our on-going  
432 and future research will apply this modeling scheme to different vegetation functional types.  
433 More importantly, most approaches have assumed that the sunlit upper canopy is the major  
434 contributor and regulator of GPP/NPP, and that either the shaded component can be largely  
435 ignored or the whole system is assumed to operate in one mode (e.g., sunlit) for total canopy  
436 foliage amount defined by LAI. Our results suggest that only taking sunlit leaves into account  
437 would lead to underestimation of canopy PRI values, implying greater than actual stress levels  
438 and leading to underestimates of LUE and GPP. Previous studies have also recognized the  
439 importance of separating sunlit and shaded leaves for modeling photosynthetic activities from  
440 leaf to canopy level (Chen et al., 1999; De Pury and Farquhar, 1997; Wang and Leuning, 1998)  
441 mostly due to the nonlinear response of leaf carbon assimilation to light intensity. Adding  
442 spectral information about the shaded canopy foliage is critical for improving our understanding  
443 about canopy physiological processes, and our ability to simulate PRI and related parameters.

444 Improvement in understanding PRI information will potentially reduce uncertainties in LUE  
445 estimates using remote sensing observations and advance carbon uptake monitoring capabilities.

446

## 447 **5. SUMMARY**

448 In this study, we examined the capability of coupling *in situ* leaf optical properties and  
449 ACRM to simulate canopy level PRI at various growth stages of a corn crop. ACRM-simulated  
450 canopy PRI values were closer to field measurements when both sunlit and shaded leaves were  
451 utilized in the scheme. The performance of the model was greatly improved when the crop was  
452 dominated by green foliage during the vegetative and mature reproductive stages. The least  
453 satisfactory results were found when the corn crop reached the senescent stage. The significance  
454 of taking both sunlit and shaded leaf segments into account for canopy PRI studies was  
455 presented. We further examined how variable sunlit/shaded canopy ratios affected the modeled  
456 results. Simulated canopy PRI values increased as the contribution from the shaded fraction  
457 increased (i.e., the sunlit/shaded ratio decreased). The analysis suggested that canopy structure  
458 information might be needed to improve simulations or to interpret PRI. These findings also  
459 imply that canopy PRI investigations and simulations should be investigated for more plant  
460 functional types.

461

## 462 **ACKNOWLEDGEMENTS**

463 This study was supported by a NASA ROSES project (PI, E.M. Middleton) funded through the  
464 Carbon Cycle Science Program (Diane Wickland, manager). The authors gratefully acknowledge  
465 A. Kuusk for sharing computer code for the canopy reflectance model, and K.F. Huemmrich  
466 (UMBC), P.K.E. Campbell (UMBC), A. Russ (USDA-ARS Hydrology and Remote Sensing

467 Lab) and D. Lagomasino (FIU) for assisting field campaign and their valuable comments. The  
468 authors thank the anonymous reviewers for their very valuable suggestions and criticism.

469

470 **REFERENCES**

471 Anderson, M.C., Norman, J.M., Meyers, T.P., & Diak, G.R. (2000). An analytical model for  
472 estimating canopy transpiration and carbon assimilation fluxes based on canopy light-use  
473 efficiency. *Agricultural and Forest Meteorology*, 101 (4), 265-289.

474 Barton, C.V.M., & North, P.R.J. (2001). Remote sensing of canopy light use efficiency using the  
475 photochemical reflectance index: Model and sensitivity analysis. *Remote Sensing of*  
476 *Environment*, 78 (3), 264-273.

477 Chen, J.M., Liu, J., Cihlar, J., & Goulden, M.L. (1999). Daily canopy photosynthesis model  
478 through temporal and spatial scaling for remote sensing applications. *Ecological Modelling*,  
479 124 (2-3), 99-119.

480 Cheng, Y.-B., Middleton, E.M., Hilker, T., Coops, N.C., Krishnan, P., & Black, T.A. (2009).  
481 Dynamics of spectral bio-indicators and their correlations with light use efficiency using  
482 directional observations at a Douglas-fir forest. *Measurement Science and Technology*, 20  
483 (9), 095107.

484 Cheng, Y.-B., Middleton, E.M., Huemmrich, K.F., Zhang, Q., Campbell, P.K.E., Corp, L.A.,  
485 Russ, A.L., & Kustas, W.P. (2010). Utilizing *in situ* directional hyperspectral measurements  
486 to validate bio-indicator simulations for a corn crop canopy. *Ecological Informatics*, 5 (5),  
487 330-338.

488 Cheng, Y.-B., Middleton, E.M., Huemmrich, K.F., Zhang, Q., Corp, L., Campbell, P., & Kustas,  
489 W. (2011). Spectral bio-indicator simulations for tracking photosynthetic activities in a corn  
490 field. *In, SPIE Optics and Photonics 2011*. San Diego, CA, USA. 21-25 August 2011.

491 Cheng, Y.-B., Zarco-Tejada, P.J., Riano, D., Rueda, C.A., & Ustin, S.L. (2006). Estimating  
492 vegetation water content with hyperspectral data for different canopy scenarios:  
493 Relationships between AVIRIS and MODIS indexes. *Remote Sensing of Environment*, 105  
494 (4), 354-366.

495 Ciganda, V., Gitelson, A., & Schepers, J. (2008). Vertical profile and temporal variation of  
496 chlorophyll in maize canopy: Quantitative “crop vigor” indicator by means of reflectance-  
497 based techniques. *Agronomy Journal*, 100 (5), 1409-1417.

498 Coops, N.C., Hilker, T., Hall, F.G., Nichol, C.J., & Drolet, G.G. (2010). Estimation of Light-use  
499 Efficiency of Terrestrial Ecosystems from Space: A Status Report. *Bioscience*, 60 (10), 788-  
500 797.

501 De Pury, D.G.G., & Farquhar, G.D. (1997). Simple scaling of photosynthesis from leaves to  
502 canopies without the errors of big-leaf models. *Plant, Cell & Environment*, 20 (5), 537-557.

503 Demmig-Adams, B., & Adams III, W.W. (1996). The role of xanthophyll cycle carotenoids in  
504 the protection of photosynthesis. *Trends in Plant Science*, 1 (1), 21-26.

505 Demmig-Adams, B., & Adams, W.W. (2000). Photosynthesis: Harvesting sunlight safely.  
506 *Nature*, 403 (6768), 371-374.

507 Drolet, G.G., Huemmrich, K.F., Hall, F.G., Middleton, E.M., Black, T.A., Barr, A.G., &  
508 Margolis, H.A. (2005). A MODIS-derived photochemical reflectance index to detect inter-  
509 annual variations in the photosynthetic light-use efficiency of a boreal deciduous forest.  
510 *Remote Sensing of Environment*, 98 (2-3), 212-224.

511 Fang, H., Liang, S., & Kuusk, A. (2003). Retrieving leaf area index using a genetic algorithm  
512 with a canopy radiative transfer model. *Remote Sensing of Environment*, 85 (3), 257-270.

513 Filella, I., Amaro, T., Araus, J.L., & Peñuelas, J. (1996). Relationship between photosynthetic  
514 radiation-use efficiency of barley canopies and the photochemical reflectance index (PRI).  
515 *Physiologia Plantarum*, 96 (2), 211-216.

516 Filella, I., Peñuelas, J., Llorens, L., & Estiarte, M. (2004). Reflectance assessment of seasonal  
517 and annual changes in biomass and CO<sub>2</sub> uptake of a Mediterranean shrubland submitted to  
518 experimental warming and drought. *Remote Sensing of Environment*, 90 (3), 308-318.

519 Gamon, J., Field, C., Fredeen, A., & Thayer, S. (2001). Assessing photosynthetic downregulation  
520 in sunflower stands with an optically-based model. *Photosynthesis Research*, 67 (1), 113-  
521 125.

522 Gamon, J.A., Field, C.B., Bilger, W., Björkman, O., Fredeen, A.L., & Peñuelas, J. (1990).  
523 Remote sensing of the xanthophyll cycle and chlorophyll fluorescence in sunflower leaves  
524 and canopies. *Oecologia*, 85 (1), 1-7.

525 Gamon, J.A., Field, C.B., Roberts, D.A., Ustin, S.L., & Valentini, R. (1993). Functional patterns  
526 in an annual grassland during an AVIRIS overflight. *Remote Sensing of Environment*, 44  
527 (2/3), 239-253.

528 Gamon, J.A., Penuelas, J., & Field, C.B. (1992). A narrow-waveband spectral index that tracks  
529 diurnal changes in photosynthetic efficiency. *Remote Sensing of Environment*, 41 (1), 35-44.

530 Gamon, J.A., Serrano, L., & Surfus, J.S. (1997). The photochemical reflectance index: an optical  
531 indicator of photosynthetic radiation use efficiency across species, functional types, and  
532 nutrient levels. *Oecologia*, 112 (4), 492-501.

533 Garbulsky, M.F., Peñuelas, J., Gamon, J., Inoue, Y., & Filella, I. (2011). The photochemical  
534 reflectance index (PRI) and the remote sensing of leaf, canopy and ecosystem radiation use  
535 efficiencies: A review and meta-analysis. *Remote Sensing of Environment*, 115 (2), 281-297.

536 Garbulsky, M.F., Peñuelas, J., Papale, D., & Filella, I. (2008). Remote estimation of carbon  
537 dioxide uptake by a Mediterranean forest. *Global Change Biology*, 14 (12), 2860-2867.

538 Gower, S.T., Kucharik, C.J., & Norman, J.M. (1999). Direct and indirect estimation of leaf area  
539 index, fAPAR, and net primary production of terrestrial ecosystems. *Remote Sensing of*  
540 *Environment*, 70 (1), 29-51.

541 Hall, F.G., Hilker, T., & Coops, N.C. (2011). PHOTOSYNSAT, photosynthesis from space:  
542 Theoretical foundations of a satellite concept and validation from tower and spaceborne data.  
543 *Remote Sensing of Environment*, 115 (8), 1918-1925.

544 Hall, F.G., Hilker, T., & Coops, N.C. (2012). Data assimilation of photosynthetic light-use  
545 efficiency using multi-angular satellite data: I. Model formulation. *Remote Sensing of*  
546 *Environment*, 121 (0), 301-308.

547 Hall, F.G., Hilker, T., Coops, N.C., Lyapustin, A., Huemmrich, K.F., Middleton, E., Margolis,  
548 H., Drolet, G., & Black, T.A. (2008). Multi-angle remote sensing of forest light use  
549 efficiency by observing PRI variation with canopy shadow fraction. *Remote Sensing of*  
550 *Environment*, 112 (7), 3201-3211.

551 Heinsch, F.A., Reeves, M.C., Votava, P., Kang, S., Milesi, C., Zhao, M., Glassy, J., Jolly, W.M.,  
552 Loehman, R., Bowker, C.F., Kimball, J.S., Nemani, R.R., & Running, S.W. (2003). User's  
553 Guide: GPP and NPP (MOD17A2/A3) Products, NASA MODIS Land Algorithm. *University*  
554 *of Montana, Missoula, MT, .*

555 Heinsch, F.A., Zhao, M., Running, S.W., Kimball, J.S., Nemani, R.R., Davis, K.J., Bolstad, P.V.,  
556 Cook, B.D., Desai, A.R., Ricciuto, D.M., Law, B.E., Oechel, W.C., Kwon, H., Luo, H.,  
557 Wofsy, S.C., Dunn, A.L., Munger, J.W., Baldocchi, D.D., Xu, L., Hollinger, D.Y.,  
558 Richardson, A.D., Stoy, P.C., Siqueira, M.B.S., Monson, R.K., Burns, S.P., & Flanagan, L.B.  
559 (2006). Evaluation of remote sensing based terrestrial productivity from MODIS using  
560 regional tower eddy flux network observations. *IEEE Transactions on Geoscience and*  
561 *Remote Sensing*, 44 (7), 1908-1925.

562 Hernández-Clemente, R., Navarro-Cerrillo, R.M., Suárez, L., Morales, F., & Zarco-Tejada, P.J.  
563 (2011). Assessing structural effects on PRI for stress detection in conifer forests. *Remote*  
564 *Sensing of Environment*, 115 (9), 2360-2375.

565 Hilker, T., Coops, N.C., Hall, F.G., Black, T.A., Chen, B., Krishnan, P., Wulder, M.A., Sellers,  
566 P.J., Middleton, E.M., & Huemmrich, K.F. (2008a). A modeling approach for upscaling  
567 gross ecosystem production to the landscape scale using remote sensing data. *Journal of*  
568 *Geophysical Research - Biogeosciences*, 113 G03006.

569 Hilker, T., Coops, N.C., Hall, F.G., Black, T.A., Wulder, M.A., Nesic, Z., & Krishnan, P.  
570 (2008b). Separating physiologically and directionally induced changes in PRI using BRDF  
571 models. *Remote Sensing of Environment*, 112 (6), 2777-2788.

572 Hilker, T., Coops, N.C., Hall, F.G., Nichol, C.J., Lyapustin, A., Black, T.A., Wulder, M.A.,  
573 Leuning, R., Barr, A., Hollinger, D.Y., Munger, B., & Tucker, C.J. (2011). Inferring  
574 terrestrial photosynthetic light use efficiency of temperate ecosystems from space. *J.*  
575 *Geophys. Res.*, 116 (G3), G03014.

576 Hilker, T., Hall, F.G., Tucker, C.J., Coops, N.C., Black, T.A., Nichol, C.J., Sellers, P.J., Barr, A.,  
577 Hollinger, D.Y., & Munger, J.W. (2012). Data assimilation of photosynthetic light-use

578 efficiency using multi-angular satellite data: II Model implementation and validation. *Remote*  
579 *Sensing of Environment*, 121 (0), 287-300.

580 Houborg, R., Anderson, M., & Daughtry, C. (2009). Utility of an image-based canopy  
581 reflectance modeling tool for remote estimation of LAI and leaf chlorophyll content at the  
582 field scale. *Remote Sensing of Environment*, 113 (1), 259-274.

583 Houborg, R., Anderson, M.C., Daughtry, C.S.T., Kustas, W.P., & Rodell, M. (2011). Using leaf  
584 chlorophyll to parameterize light-use-efficiency within a thermal-based carbon, water and  
585 energy exchange model. *Remote Sensing of Environment*, 115 (7), 1694-1705.

586 Huemmrich, K.F., Middleton, E.M., Landis, D., Black, T.A., B., A., McCaughey, J.H., & Hall,  
587 F.G. (2009). Remote sensing of light use efficiency. In, *Proceedings of the 30th Canadian*  
588 *Symposium on Remote Sensing*. Lethbridge, Alberta, Canada. June 22-25, 2009.

589 Inoue, Y., Peñuelas, J., Miyata, A., & Mano, M. (2008). Normalized difference spectral indices  
590 for estimating photosynthetic efficiency and capacity at a canopy scale derived from  
591 hyperspectral and CO<sub>2</sub> flux measurements in rice. *Remote Sensing of Environment*, 112 (1),  
592 156-172.

593 Jacquemoud, S. (1993). Inversion of the PROSPECT + SAIL canopy reflectance model from  
594 AVIRIS equivalent spectra: Theoretical study. *Remote Sensing of Environment*, 44 (2/3),  
595 281-292.

596 Jacquemoud, S., Ustin, S.L., Verdebout, J., Schmuck, G., Andreoli, G., & Hosgood, B. (1996).  
597 Estimating leaf biochemistry using the PROSPECT leaf optical properties model. *Remote*  
598 *Sensing of Environment*, 56 (3), 194-202.

599 King, D.A., Turner, D.P., & Ritts, W.D. (2011). Parameterization of a diagnostic carbon cycle  
600 model for continental scale application. *Remote Sensing of Environment*, 115 (7), 1653-1664.

601 Kuusk, A. (1995a). A fast, invertible canopy reflectance model. *Remote Sensing of Environment*,  
602 51 (3), 342-350.

603 Kuusk, A. (1995b). A Markov chain model of canopy reflectance. *Agricultural and Forest*  
604 *Meteorology*, 76 (3-4), 221-236.

605 Kuusk, A. (2001). A two-layer canopy reflectance model. *Journal of Quantitative Spectroscopy*  
606 *and Radiative Transfer*, 71 (1), 1-9.

607 Law, B.E., & Waring, R.H. (1994). Combining remote sensing and climatic data to estimate net  
608 primary production across Oregon. *Ecological Applications*, 4 (4), 717-728.

609 Lin, J.C., Pejam, M.R., Chan, E., Wofsy, S.C., Gottlieb, E.W., Margolis, H.A., & McCaughey,  
610 J.H. (2011). Attributing uncertainties in simulated biospheric carbon fluxes to different error  
611 sources. *Global Biogeochemical Cycles (in press)*

612 Mahadevan, P., Wofsy, S.C., Matross, D.M., Xiao, X., Dunn, A.L., Lin, J.C., Gerbig, C.,  
613 Munger, J.W., Chow, V.Y., & Gottlieb, E.W. (2008). A satellite-based biosphere  
614 parameterization for net ecosystem CO<sub>2</sub> exchange: Vegetation Photosynthesis and  
615 Respiration Model (VPRM). *Global Biogeochem. Cycles*, 22 (2), GB2005.

616 Middleton, E.M., Cheng, Y.-B., Hilker, T., Black, T.A., Krishnan, P., Coops, N.C., &  
617 Huemmrich, K.F. (2009). Linking foliage spectral responses to canopy level ecosystem  
618 photosynthetic light use efficiency at a Douglas-fir forest in Canada. *Canadian Journal of*  
619 *Remote Sensing*, 35 ( 2), 166-188.

620 Middleton, E.M., Huemmrich, K.F., Cheng, Y.-B., & Margolis, H.A. (2011). Spectral  
621 bioindicators of photosynthetic efficiency and vegetation stress. In P.S. Thenkabail, J.G.  
622 Lyon & A. Huete (Eds.), *Hyperspectral Remote Sensing of Vegetation* (pp. 265-288): CRC  
623 Press.

624 Monteith, J.L. (1972). Solar-radiation and productivity in tropical ecosystems. *Journal of Applied*  
625 *Ecology*, 9 (3), 747-766.

626 Monteith, J.L. (1977). Climate and the efficiency of crop production in Britain. *Philosophical*  
627 *Transaction of the Royal Society of London. Series B: Biological Sciences*, 281 (980), 277-  
628 294.

629 Müller, P., Li, X.-P., & Niyogi, K.K. (2001). Non-photochemical quenching. A response to  
630 excess light energy. *Plant Physiology*, 125 (4), 1558-1566.

631 Nichol, C.J., & Grace, J. (2010). Determination of leaf pigment content in *Calluna vulgaris*  
632 shoots from spectral reflectance. *International Journal of Remote Sensing*, 31 (20), 5409-  
633 5422.

634 Nichol, C.J., Lloyd, J., Shibistova, O., Arneth, A., Röser, C., Knohl, A., Matsubara, S., & Grace,  
635 J. (2002). Remote sensing of photosynthetic-light-use efficiency of a Siberian boreal forest.  
636 *Tellus*, 54B (5), 677-687.

637 Peñuelas, J., Filella, I., & Gamon, J.A. (1995). Assessment of photosynthetic radiation-use  
638 efficiency with spectral reflectance. *New Phytologist*, 131 (3), 291-296.

639 Peñuelas, J., Garbulsky, M.F., & Filella, I. (2011). Photochemical reflectance index (PRI) and  
640 remote sensing of plant CO<sub>2</sub> uptake. *New Phytologist*, 191 (3), 596-599.

641 Peñuelas, J., & Inoue, Y. (2000). Reflectance assessment of canopy CO<sub>2</sub> uptake. *International*  
642 *Journal of Remote Sensing*, 21 (17), 3353-3356.

643 Peñuelas, J., Llusia, J., Pinol, J., & Filella, I. (1997). Photochemical reflectance index and leaf  
644 photosynthetic radiation-use-efficiency assessment in Mediterranean trees. *International*  
645 *Journal of Remote Sensing*, 18 (13), 2863-2868.

646 Pfündel, E.E., & Bilger, W. (1994). Regulation and possible function of the violaxanthin cycle.  
647 *Photosynthesis Research*, 42 (2), 89-109.

648 Prince, S.D., & Goward, S.N. (1995). Global primary production: A remote sensing approach.  
649 *Journal of Biogeography*, 22 (4-5), 815-835.

650 Sims, D.A., & Gamon, J.A. (2002). Relationships between leaf pigment content and spectral  
651 reflectance across a wide range of species, leaf structures and developmental stages. *Remote*  
652 *Sensing of Environment*, 81 (2-3), 337-354.

653 Sims, D.A., Luo, H., Hastings, S., Oechel, W.C., Rahman, A.F., & Gamon, J.A. (2006). Parallel  
654 adjustments in vegetation greenness and ecosystem CO<sub>2</sub> exchange in response to drought in  
655 a Southern California chaparral ecosystem. *Remote Sensing of Environment*, 103 (3), 289-  
656 303.

657 Stylinski, Gamon, & Oechel (2002). Seasonal patterns of reflectance indices, carotenoid  
658 pigments and photosynthesis of evergreen chaparral species. *Oecologia*, 131 (3), 366-374.

659 Suárez, L., Zarco-Tejada, P.J., Berni, J.A.J., González-Dugo, V., & Fereres, E. (2009).  
660 Modelling PRI for water stress detection using radiative transfer models. *Remote Sensing of*  
661 *Environment*, 113 (4), 730-744.

662 Verhoef, W. (1984). Light scattering by leaf layers with application to canopy reflectance  
663 modeling: The SAIL model. *Remote Sensing of Environment*, 16 (2), 125-141.

664 Wang, Y.P., & Leuning, R. (1998). A two-leaf model for canopy conductance, photosynthesis  
665 and partitioning of available energy I: Model description and comparison with a multi-  
666 layered model. *Agricultural and Forest Meteorology*, 91 (1-2), 89-111.

667 Xiao, X., Zhang, Q., Braswell, B., Urbanski, S., Boles, S., Wofsy, S., Moore III, B., & Ojima, D.  
668 (2004). Modeling gross primary production of temperate deciduous broadleaf forest using  
669 satellite images and climate data. *Remote Sensing of Environment*, 91 (2), 256-270.

670 Zarco-Tejada, P.J., Rueda, C.A., & Ustin, S.L. (2003). Water content estimation in vegetation  
671 with MODIS reflectance data and model inversion methods. *Remote Sensing of Environment*,  
672 85 (1), 109-124.

673 Zhang, Q., Middleton, E.M., Gao, B.-C., & Cheng, Y.-B. (2011). Using EO-1 Hyperion to  
674 simulate HypIRI products for a coniferous forest: the fraction of PAR absorbed by  
675 chlorophyll (fAPARchl) and leaf water content (LWC). *Geoscience and Remote Sensing*,  
676 *IEEE Transactions on*, 50(5), 1844-1852.

677

678

679 **FIGURE CAPTIONS**

680 **Figure 1.** PRI values derived from *in situ* leaf reflectance for the sunlit ( $\square$ ) and shaded ( $\blacksquare$ )  
681 leaves used as input data in the simulations and daily average ( $\blacksquare$ ) on three field days in 2010.  
682 Values are shown as mean  $\pm$  SE.

683 **Figure 2.** *In situ* canopy PRI values from field measurements are shown for nadir ( $\theta_v=0^\circ$ ;  $\psi=0^\circ$ )  
684 and for three additional view zenith angles ( $\theta_v=30^\circ, 45^\circ, 60^\circ$ ) which were coupled with eight  
685 relative azimuth angles ( $\psi=0^\circ$  to  $315^\circ$  with  $45^\circ$  increment) on July 1<sup>st</sup> ( $\blacksquare$ ), July 15<sup>th</sup> ( $\blacksquare$ ), and  
686 August 9<sup>th</sup> ( $\square$ ) in 2010. Values are shown as mean  $\pm$  SE. The mature canopy was clearly  
687 differentiated from early and late canopies, with higher PRI values at any  $\theta_v$ . Early and late  
688 growth stages were similar at  $\theta_v = 30^\circ$  and  $45^\circ$ , but were differentiated at  $\theta_v = 60^\circ$ . These results  
689 were used as validation data for simulations.

690 **Figure 3.** Comparisons and regressions between simulated and *in situ* PRI values on three days  
691 during the 2010 growing season: (a)(b) July 1; (c)(d) July 15; and (e)(f) August 9. Simulations  
692 were performed using either sunlit leaves only ( $\diamond$ ) or both sunlit and shaded leaves ( $\blacktriangle$ ). Values  
693 are shown as mean  $\pm$  SE. in (a)(c)(e). In general, simulations agreed with field observations  
694 when both sunlit and shaded foliage were included.

695 **Figure 4.** Summary chart of statistics representing all data collected on the three 2010 field  
696 dates, for simulations using either sunlit canopy only or both sunlit and shaded canopy sectors:  
697 (a) correlation coefficient ( $r$ ) and (b) root mean square error (RMSE) relating *in situ* and  
698 simulated PRI values.

699 **Figure 5.** Differences between values for *in situ* versus simulated PRI plotted against viewing  
700 geometry ( $\theta_v$  and  $\psi$ ) for the three growth stages in 2010. The black dashed line indicates zero

701 difference between *in situ* and simulated values. Discrepancies indicate the error incurred in  
702 simulations.

703 **Figure 6.** Changes in PRI values when 2-layer simulations were performed with various  
704 sunlit/shaded canopy ratios, where the upper layer is sunlit and the lower layer is shaded.  
705 Simulations were done using parameters from the mature and green VT canopy, LAI = 2.48 on  
706 July 15, 2010. Six sunlit/shaded ratio cases were investigated, as shown in the label, represented  
707 by increasingly darker grey tone as more shaded leaves are included. The nadir case is included  
708 in the top panel.

709 **Figure 7.** Correlations between *in situ* PRI measurements and PRI values simulated using  
710 various sunlit/shaded canopy ratios, for the mature VT canopy on July 15, 2010. LAI = 2.48.

711 **Figure 8.** Statistics for the correlation coefficient ( $r$ ) and root mean square error (RMSE),  
712 relating *in situ* PRI measurements and simulated PRI values across various sunlit/shaded canopy  
713 ratios. Based on the VT canopy (July 15, 2010; LAI = 2.48).

714 **Figure 9.** Parameters of the regression line ( $y=ax+b$ ) relating *in situ* and simulated PRI values,  
715 using various sunlit/shaded canopy ratios. Parameter “a” is the slope while “b” is the offset of the  
716 regression line. Based on the VT canopy (July 15, 2010; LAI = 2.48).

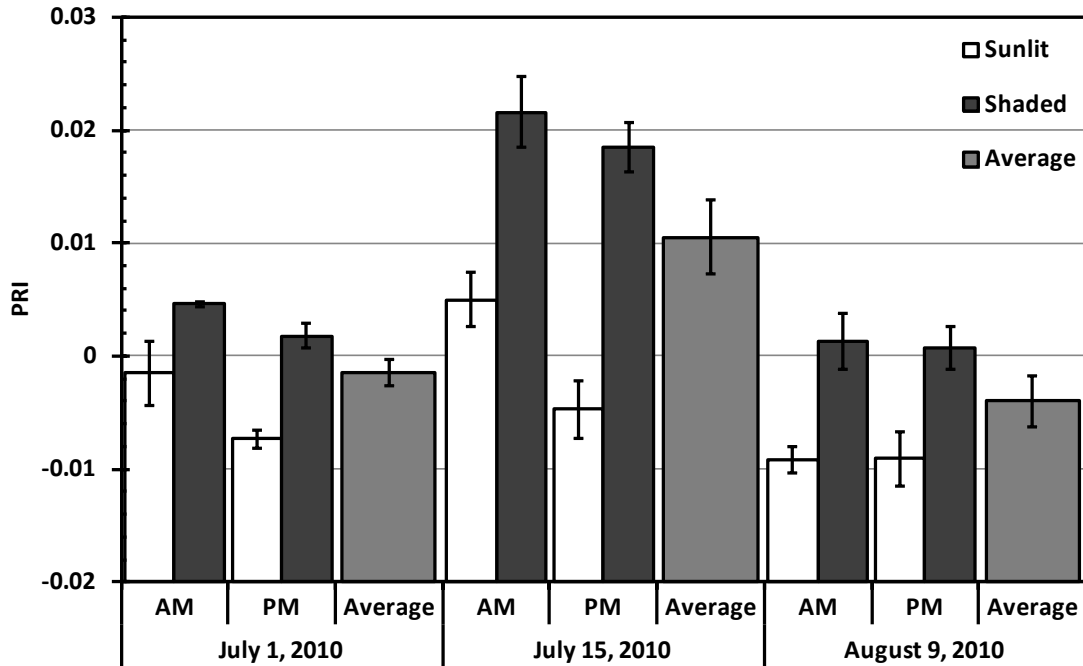
717

## 718 **TABLE CAPTIONS**

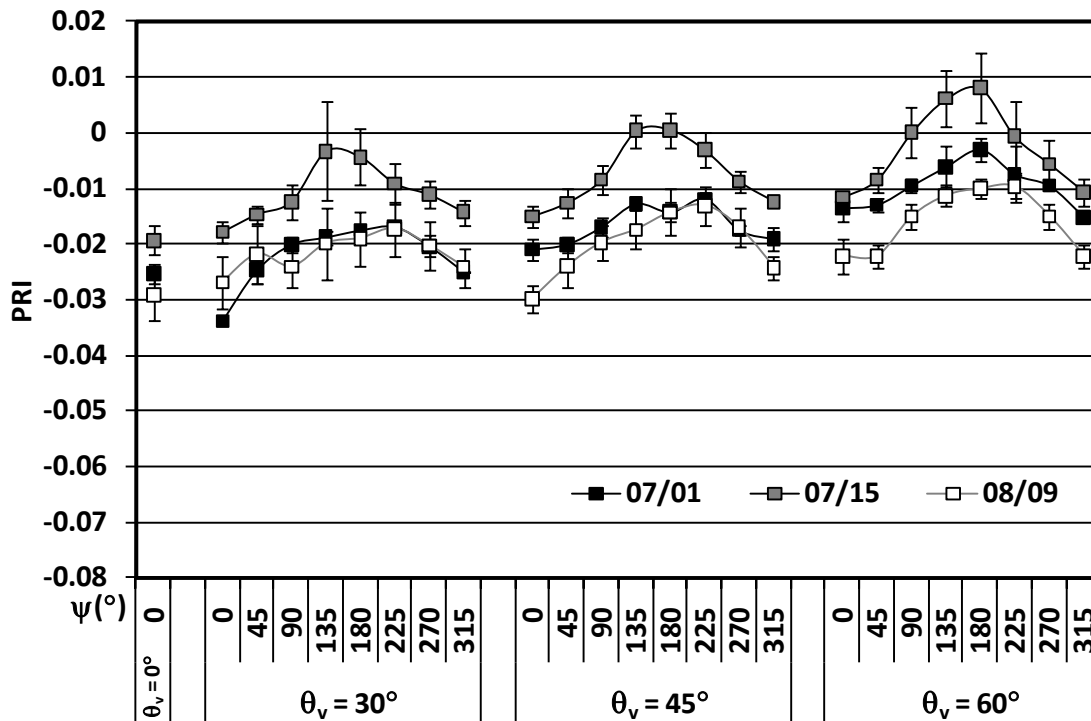
719 **Table 1.** Value or range of parameters used as input to ACRM in this study.

720 **Table 2.** Correlation coefficients ( $r$ ) and root mean square errors (RMSE) relating *in situ* PRI  
721 measurements and ACRM-simulated PRI values using various sunlit/shaded canopy ratios are  
722 presented for three additional days: an early 2008 growth stage and two 2010 growth stages.

723



724  
 725 **Figure 1.** PRI values derived from *in situ* leaf reflectance for the sunlit (□) and shaded (■)  
 726 leaves used as input data in the simulations and daily average (■) on three field days in 2010.  
 727 Values are shown as mean ± SE.



729

730

731

732

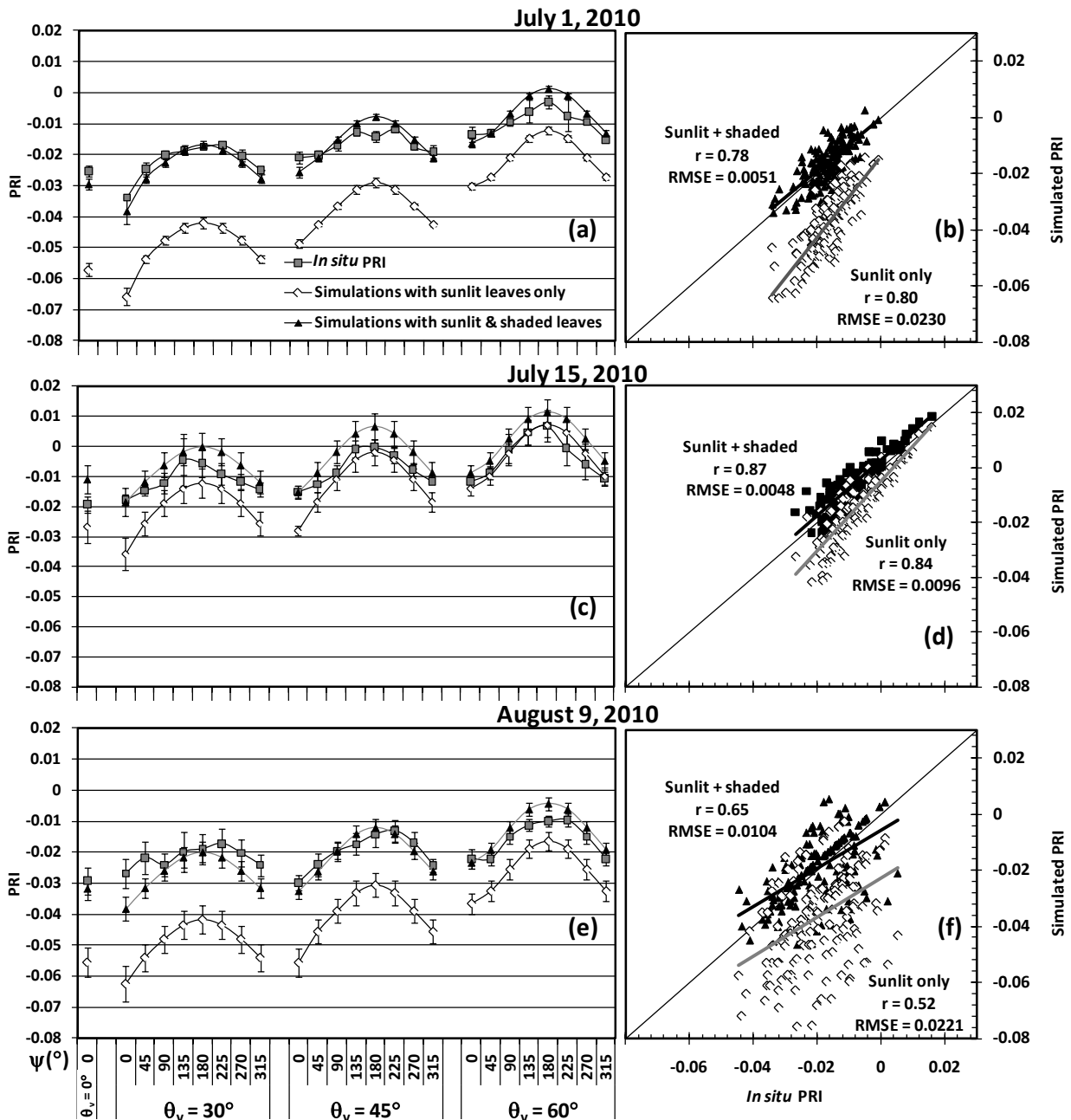
733

734

735

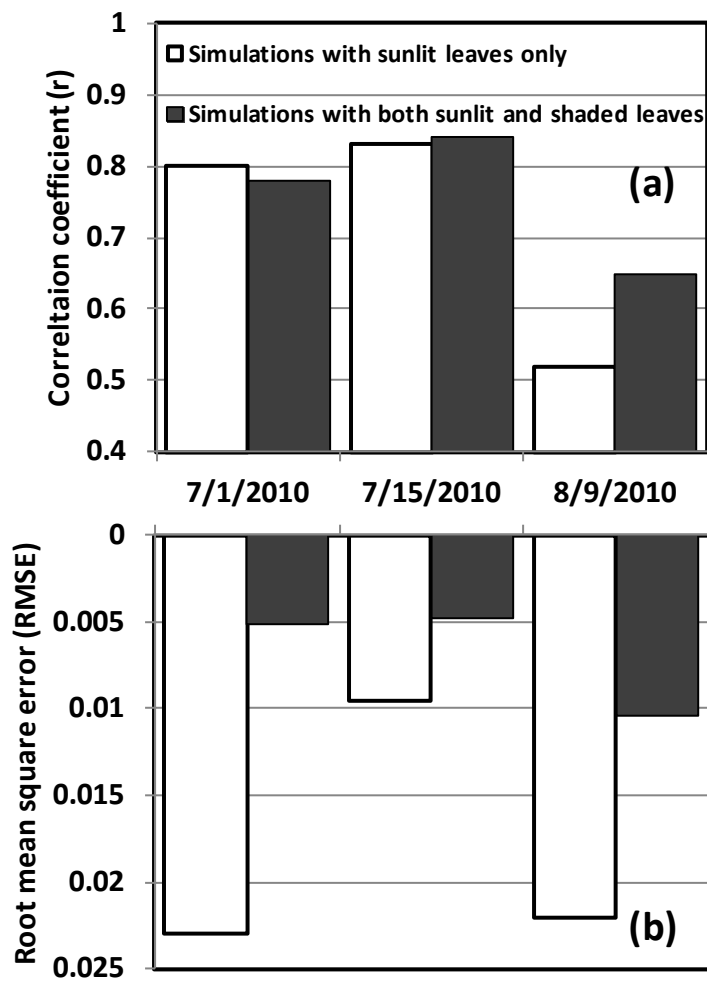
736

**Figure 2.** *In situ* canopy PRI values from field measurements are shown for nadir ( $\theta_v=0^\circ$ ;  $\psi=0^\circ$ ) and for three additional view zenith angles ( $\theta_v=30^\circ, 45^\circ, 60^\circ$ ) which were coupled with eight relative azimuth angles ( $\psi=0^\circ$  to  $315^\circ$  with  $45^\circ$  increment) on July 1<sup>st</sup> (■), July 15<sup>th</sup> (■), and August 9<sup>th</sup> (□) in 2010. Values are shown as mean  $\pm$  SE. The mature canopy was clearly differentiated from early and late canopies, with higher PRI values at any  $\theta_v$ . Early and late growth stages were similar at  $\theta_v = 30^\circ$  and  $45^\circ$ , but were differentiated at  $\theta_v = 60^\circ$ . These results were used as validation data for simulations.

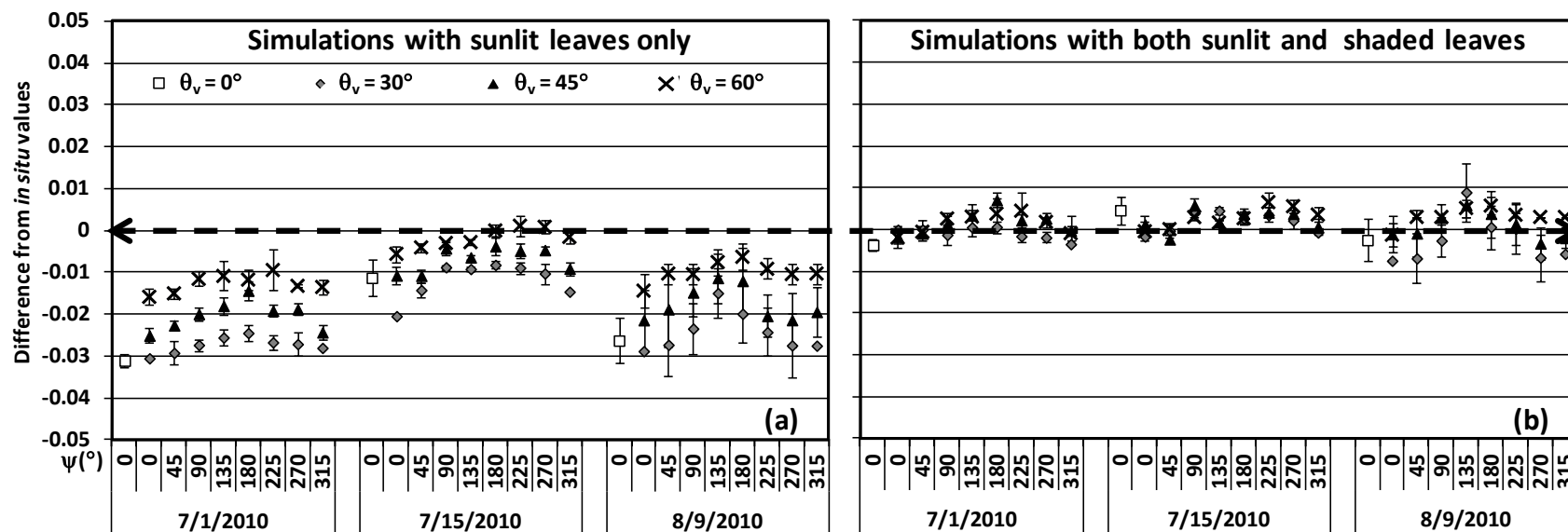


738  
739  
740  
741  
742  
743

**Figure 3.** Comparisons and regressions between simulated and *in situ* PRI values on three days during the 2010 growing season: (a)(b) July 1; (c)(d) July 15; and (e)(f) August 9. Simulations were performed using either sunlit leaves only ( $\diamond$ ) or both sunlit and shaded leaves ( $\blacktriangle$ ). Values are shown as mean  $\pm$  SE. in (a)(c)(e). In general, simulations agreed with field observations when both sunlit and shaded foliage were included.



744  
 745 **Figure 4.** Summary chart of statistics representing all data collected on the three 2010 field  
 746 dates, for simulations using either sunlit canopy only or both sunlit and shaded canopy sectors:  
 747 (a) correlation coefficient (r) and (b) root mean square error (RMSE) relating *in situ* and  
 748 simulated PRI values.



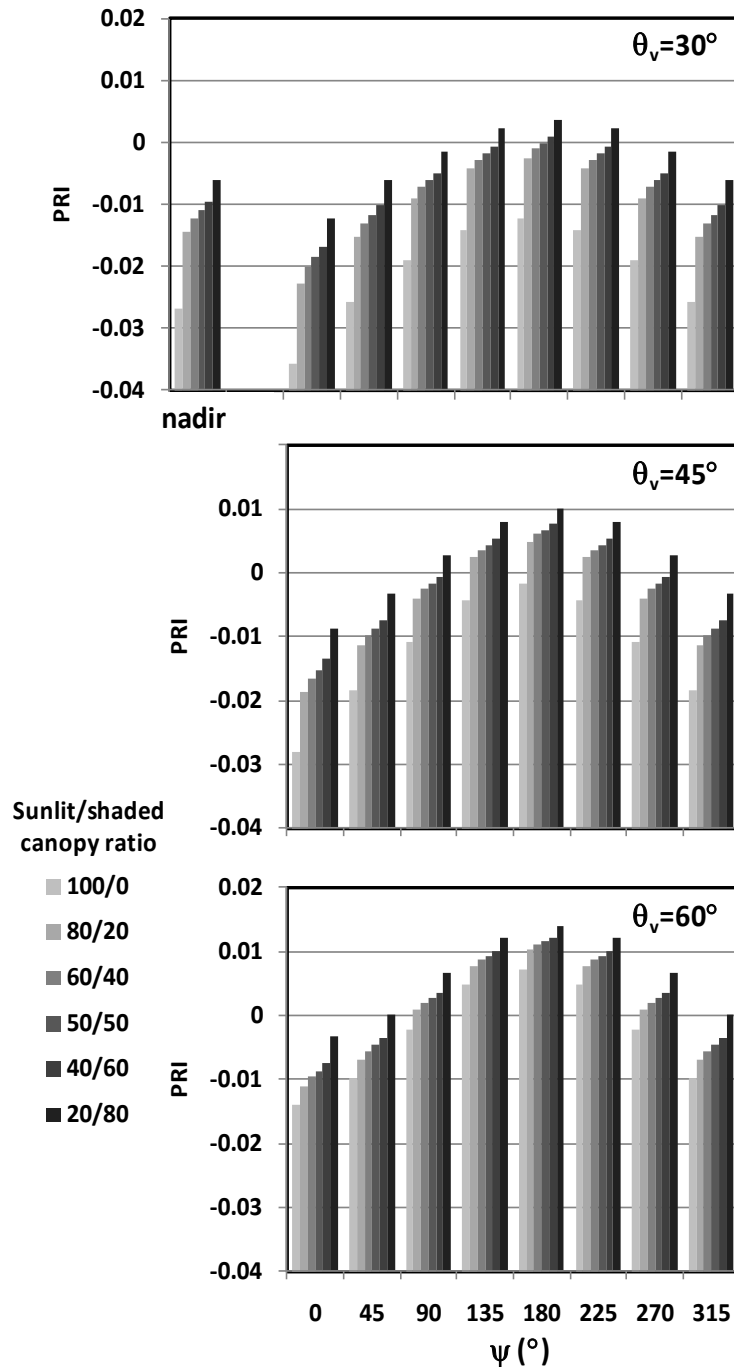
750

751

752

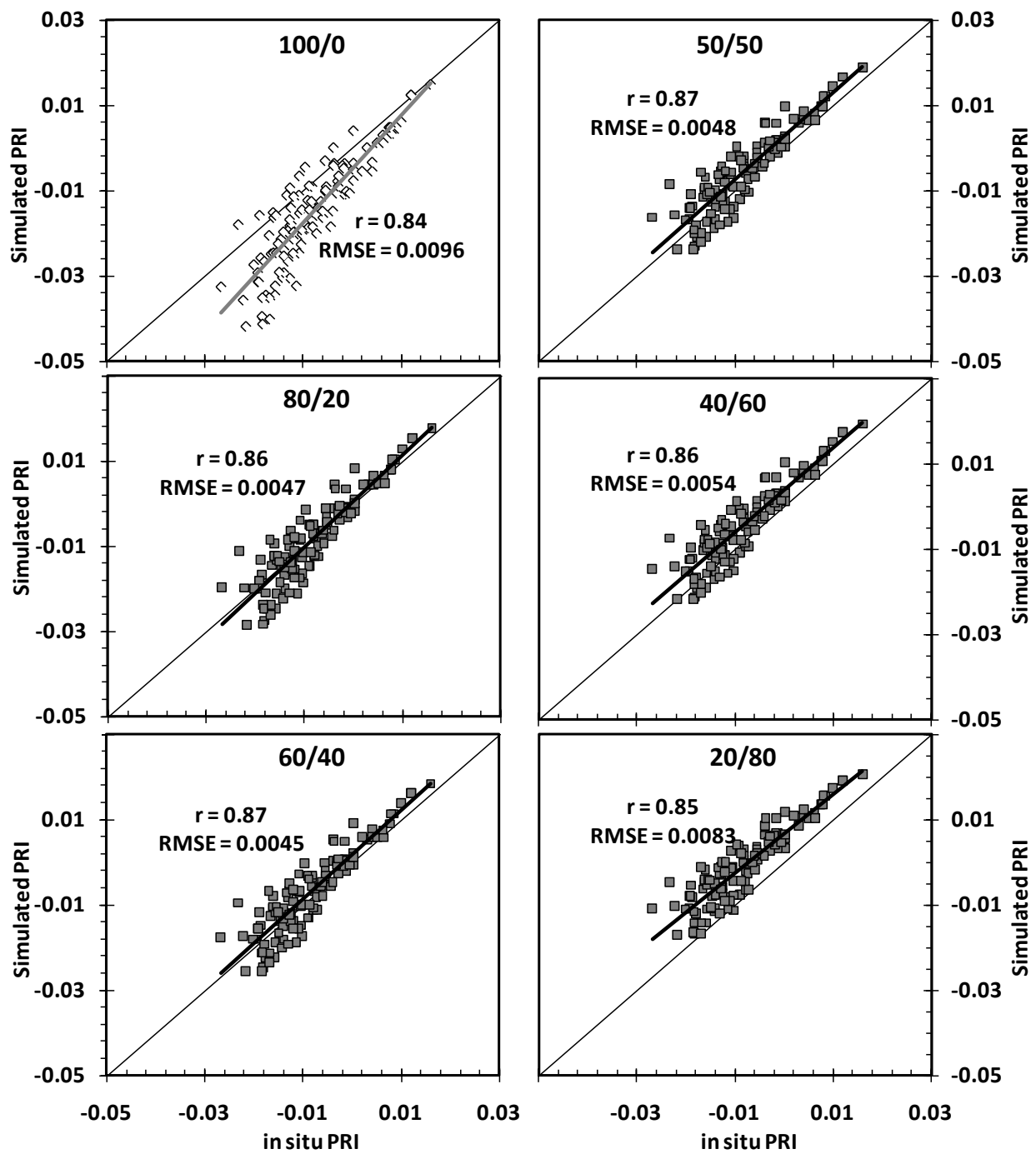
753

**Figure 5.** Differences between values for *in situ* versus simulated PRI plotted against viewing geometry ( $\theta_v$  and  $\psi$ ) for the three growth stages in 2010. The black dashed line indicates zero difference between *in situ* and simulated values. Discrepancies indicate the error incurred in simulations.



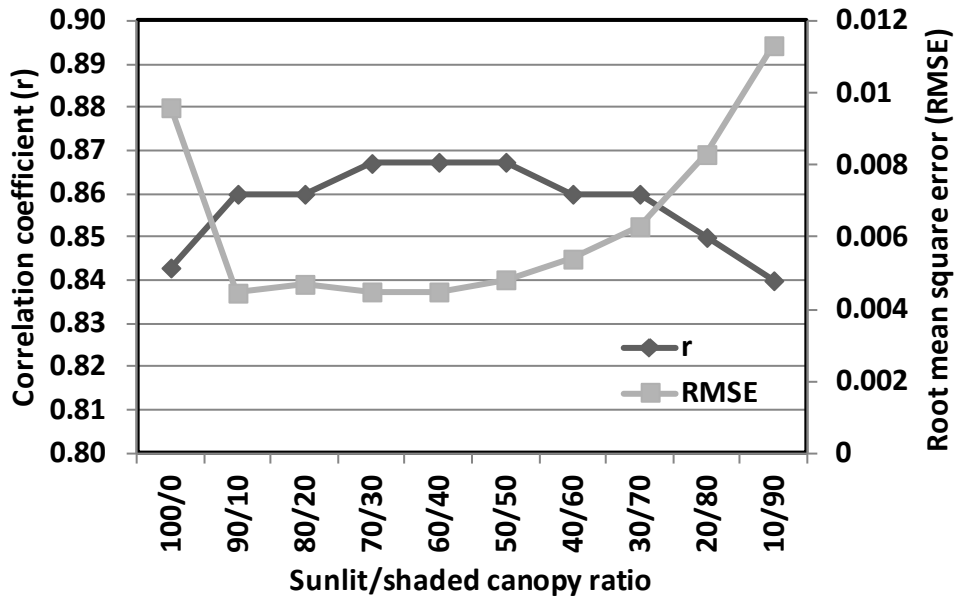
754  
755  
756  
757  
758  
759  
760

**Figure 6.** Changes in PRI values when 2-layer simulations were performed with various sunlit/shaded canopy ratios, where the upper layer is sunlit and the lower layer is shaded. Simulations were done using parameters from the mature and green VT canopy, LAI = 2.48 on July 15, 2010. Six sunlit/shaded ratio cases were investigated, as shown in the label, represented by increasingly darker grey tone as more shaded leaves are included. The nadir case is included in the top panel.

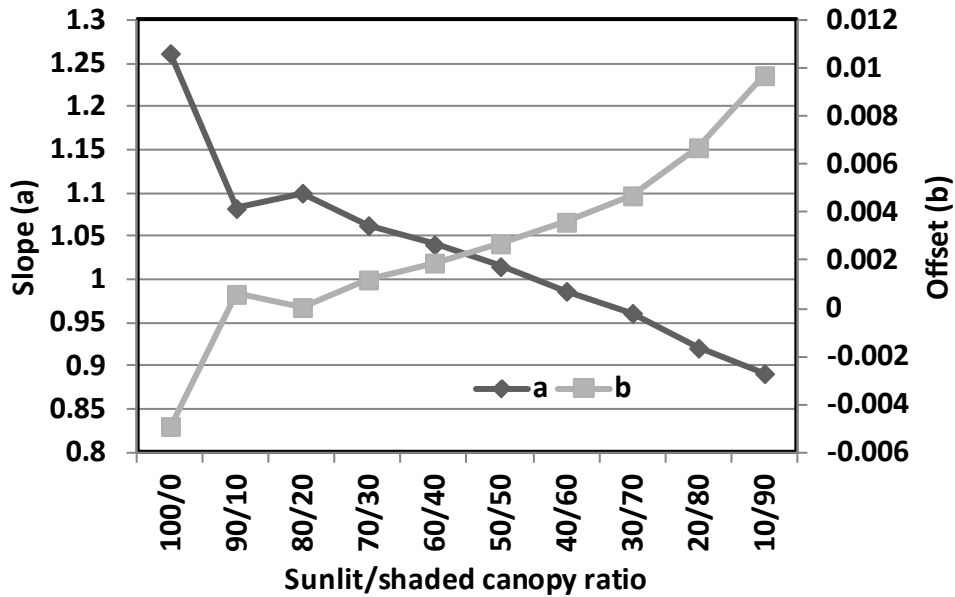


761  
762  
763

**Figure 7.** Correlations between *in situ* PRI measurements and PRI values simulated using various sunlit/shaded canopy ratios, for the mature VT canopy on July 15, 2010. LAI = 2.48.



764  
 765 **Figure 8.** Statistics for the correlation coefficient (r) and root mean square error (RMSE),  
 766 relating *in situ* PRI measurements and simulated PRI values across various sunlit/shaded canopy  
 767 ratios. Based on the VT canopy (July 15, 2010; LAI = 2.48).  
 768



769  
 770 **Figure 9.** Parameters of the regression line ( $y=ax+b$ ) relating *in situ* and simulated PRI values,  
 771 using various sunlit/shaded canopy ratios. Parameter “a” is the slope while “b” is the offset of the  
 772 regression line. Based on the VT canopy (July 15, 2010; LAI = 2.48).

773 **Table 1.** Value or range of parameters used as input to ACRM in this study.

Date	July 1, 2010	July 15, 2010	August 9, 2010
LAI	1.92	2.48	1.81
Solar zenith angle ( $\theta_s$ )	16.6° to 42.8°	18.1° to 45.3°	24.1° to 51.2°
View zenith angle ( $\theta_v$ )	0°, 30°, 45°, 60°		
Relative azimuth angle ( $\psi$ )	0° to 315° at 45° increments		
Relative leaf size	0.15		
Markov parameter	1.0		
Leaf angle distribution parameter	$\varepsilon = 0; \theta_m = 0$		

774  
775  
776  
777  
778

**Table 2.** Correlation coefficients (r) and root mean square errors (RMSE) relating *in situ* PRI measurements and ACRM-simulated PRI values using various sunlit/shaded canopy ratios are presented for three additional days: an early 2008 growth stage and two 2010 growth stages.

		100/0	80/20	60/40	50/50	40/60	20/80
August 1, 2008	r	0.71	0.80	0.85	0.86	0.84	0.82
	RMSE	0.019	0.009	0.006	0.004	0.006	0.007
July 1, 2010	r	0.80	0.77	0.78	0.78	0.75	0.68
	RMSE	0.023	0.010	0.007	0.005	0.006	0.007
August 9,2010	r	0.52	0.57	0.62	0.65	0.65	0.64
	RMSE	0.022	0.014	0.010	0.010	0.011	0.012

779  
780